

ACCEPTED MANUSCRIPT

Large room-temperature magnetoresistance in van der Waals ferromagnet/semiconductor junctions

To cite this article before publication: Wenkai Zhu *et al* 2022 *Chinese Phys. Lett.* in press <https://doi.org/10.1088/0256-307X/39/12/128501>

Manuscript version: Accepted Manuscript

Accepted Manuscript is “the version of the article accepted for publication including all changes made as a result of the peer review process, and which may also include the addition to the article by IOP Publishing of a header, an article ID, a cover sheet and/or an ‘Accepted Manuscript’ watermark, but excluding any other editing, typesetting or other changes made by IOP Publishing and/or its licensors”

This Accepted Manuscript is © 2022 Chinese Physical Society and IOP Publishing Ltd.

During the embargo period (the 12 month period from the publication of the Version of Record of this article), the Accepted Manuscript is fully protected by copyright and cannot be reused or reposted elsewhere.

As the Version of Record of this article is going to be / has been published on a subscription basis, this Accepted Manuscript is available for reuse under a CC BY-NC-ND 3.0 licence after the 12 month embargo period.

After the embargo period, everyone is permitted to use copy and redistribute this article for non-commercial purposes only, provided that they adhere to all the terms of the licence <https://creativecommons.org/licenses/by-nc-nd/3.0>

Although reasonable endeavours have been taken to obtain all necessary permissions from third parties to include their copyrighted content within this article, their full citation and copyright line may not be present in this Accepted Manuscript version. Before using any content from this article, please refer to the Version of Record on IOPscience once published for full citation and copyright details, as permissions will likely be required. All third party content is fully copyright protected, unless specifically stated otherwise in the figure caption in the Version of Record.

View the [article online](#) for updates and enhancements.

**Large room-temperature magnetoresistance in van der Waals
ferromagnet/semiconductor junctions**

Wenkai Zhu^{1,2,†}, Shihong Xie^{1,3,†}, Hailong Lin^{1,2,†}, Gaojie Zhang^{4,5}, Hao Wu^{4,5}, Tiangui Hu^{1,2},
Ziao Wang^{1,2}, Xiaomin Zhang^{1,2}, Jiahan Xu¹, Yujing Wang^{1,2}, Yuanhui Zheng¹, Faguang Yan¹,
Jing Zhang¹, Lixia Zhao^{1,6}, Amalia Patané³, Jia Zhang^{5,7}, Haixin Chang^{4,5,*}, Kaiyou Wang^{1,2,*}

¹State Key Laboratory of Superlattices and Microstructures, Institute of Semiconductors, Chinese Academy of Sciences, Beijing 100083, China

²Center of Materials Science and Optoelectronics Engineering, University of Chinese Academy of Sciences, Beijing 100049, China

³School of Physics and Astronomy, University of Nottingham, Nottingham NG7 2RD, United Kingdom

⁴Center for Joining and Electronic Packaging, State Key Laboratory of Material Processing and Die & Mold Technology, School of Materials Science and Engineering, Huazhong University of Science and Technology, Wuhan 430074, China

⁵Wuhan National High Magnetic Field Center, Huazhong University of Science and Technology, Wuhan 430074, China

⁶School of Electrical and Electronic Engineering, Tiangong University, Tianjin 300387, China

⁷School of Physics, Huazhong University of Science and Technology, Wuhan 430074, China

†These authors contributed equally to this work.

*Authors to whom any correspondence should be addressed.

Email:

hxchang@hust.edu.cn

kywang@semi.ac.cn

Keywords: magnetic tunnel junctions, room-temperature magnetoresistance, van der Waals crystals, Fe₃GaTe₂, WSe₂

Abstract

The magnetic tunnel junction (MTJ) is the core component in memory technologies, such as the magnetic random-access memory, magnetic sensors and programmable logic devices. In particular, MTJs based on two-dimensional (2D) van der Waals (vdW) heterostructures offer unprecedented opportunities for low power consumption and miniaturization of spintronic devices. However, their operation at room temperature remains a challenge. Here, we report a large tunnel magnetoresistance (TMR) of up to 85% at room temperature ($T = 300$ K) in vdW MTJs based on a thin (< 10 nm) semiconductor spacer WSe_2 layer embedded between two Fe_3GaTe_2 electrodes with intrinsic above-room-temperature ferromagnetism. The TMR in the MTJ increases with decreasing temperature up to 164% at $T = 10$ K. The demonstration of TMR in ultra-thin MTJs at room-temperature opens a realistic and promising route for next-generation spintronic applications beyond the current state of the art.

Letter

Magnetic tunnel junctions (MTJs) with large tunnel magnetoresistance (TMR) play an important role in many technologies ranging from magnetic-field sensing and non-volatile magnetic random-access memories (MRAM) to programmable spin logic devices [1-4]. Traditional MTJs normally consist of three-dimensionally bonded ferromagnetic metals and non-magnetic wide-gap oxides, such as Fe/MgO/Fe [5-7] and NiFe/TaO/Al₂O₃/Co [8]. Different from covalently bonded multilayer systems, van der Waals (vdW) heterostructures with atomically sharp and clean interfaces offer opportunities to build high-quality junctions without the requirement of lattice matching [9, 10]. Specifically, the recent discovery of magnetic two-dimensional (2D) vdW materials, such as Cr₂Ge₂Te₆ [11], CrI₃ [12, 13], Fe₃GeTe₂ [14, 15] and Fe₅GeTe₂ [16] not only provide platforms for studies of novel physics phenomena, but also offer promising application prospects for 2D electronic devices where the spin is used as an extra degree of freedom [17-19].

Amongst the catalogue of magnetic 2D vdW materials, ferromagnet Fe₃GeTe₂ has attracted extensive attention from worldwide researchers owing to its metallic nature and strong perpendicular magnetic anisotropy (PMA) [20-29]. At low temperatures, TMRs of 41% (10 K) and 300% (4.2 K) were reported in Fe₃GeTe₂/InSe/Fe₃GeTe₂ MTJs [26] and Fe₃GeTe₂/hBN/Fe₃GeTe₂ MTJs [30], respectively. As the temperature approaches the Curie temperature of Fe₃GeTe₂ (T_C , 220 K in bulk and 130 K in monolayer), the TMR of the Fe₃GeTe₂-based MTJs quickly decreases and vanishes [25, 27, 30, 31]. Although the T_C of 2D magnets can be tuned to room temperature by electrostatic gating [15], high-pressure [32] or interlayer magnetic coupling [33], the room temperature operation of vertical MTJs under these conditions remains a challenge, hindering prospects for future applications [34]. On the other hand, there is the ambition for all-2D room-temperature MTJs to be manufactured for production within the next decade [1]. This could be facilitated the recent discovery of the vdW

crystal Fe_3GaTe_2 that has a high saturation magnetic moment, robust large PMA, and Curie temperature T_C of up to 380 K [35].

In this letter, we use Fe_3GaTe_2 as the ferromagnetic electrodes in an all-vdW MTJ. The tunnel barrier of the MTJ is the transition-metal dichalcogenide (TMDC) semiconductor WSe_2 . Due to its tunable bandgap and long spin diffusion length, WSe_2 is suitable for the construction of 2D magnetic devices, such as MTJs [27, 30] and spin field-effect transistors (FETs) [36]. Moreover, the magnetoresistance of MTJs can be tuned by the thickness of the WSe_2 spacer layer through the spin filtering effect [27]. The $\text{Fe}_3\text{GaTe}_2/\text{WSe}_2/\text{Fe}_3\text{GaTe}_2$ MTJ exhibits a TMR of 85% at room temperature ($T = 300$ K). Together with this significant achievement, we find that the operating temperature of the MTJ is up to 380 K, a record-high operating temperature amongst vdW MTJs, opening disruptive improvement towards practical applications for next-generation spintronic devices.

High-quality vdW ferromagnetic crystal Fe_3GaTe_2 is grown by the self-flux method and has a hexagonal structure of space group $P6_3/mmc$ with lattice parameters $a = b = 3.9860$ Å and $c = 16.2290$ Å ($\alpha = \beta = 90^\circ$, $\gamma = 120^\circ$) [35]. In the Fe_3GaTe_2 crystal, the Fe_3Ga heterometallic slab is sandwiched between two Te layers, and the vdW gap is between two adjacent Te atoms (Fig. 1a). Two inequivalent Fe sites are distinguished by brown and blue balls, respectively. The slabs of Fe_3GaTe_2 are stacked along the c -axis with an interlayer spacing of ~ 0.78 nm [35]. **As the magnetic moment of Ga and Te atoms in Fe_3GaTe_2 are negligible, the ferromagnetism of Fe_3GaTe_2 mainly comes from the $3d$ -orbital electrons in Fe atoms [35].** An exfoliated ~ 10 nm-thick Fe_3GaTe_2 flake was used to fabricate a Hall-bar (Fig. 1b) and investigate the magnetic properties of Fe_3GaTe_2 (fabrication details in Supplementary Note 1). The thickness of Fe_3GaTe_2 is measured by atomic force microscopy (AFM) (Fig. 1c upper-left inset). In the anomalous Hall effect (AHE) measurements, the longitudinal resistance R_{xx} increases monotonically with increasing temperature, as expected for a metallic layer (Fig. 1c). Figure 1d

depicts the temperature-dependent AHE signal R_{xy} (transverse resistance) as the perpendicular applied magnetic field B sweeps between -0.6 and $+0.6$ T. As the temperature increases from 10 to 380 K, the $R_{xy} - B$ curves display almost perfectly square-shaped hysteresis loops, indicating that the Fe_3GaTe_2 flake has strong PMA. Especially, the AHE signal of the Fe_3GaTe_2 Hall-bar is still measurable at room temperature. Due to the enhancement of the thermal fluctuations close to T_C , the coercivity also decreases monotonically with increasing temperature and nearly vanishes at 380 K. Another thicker Fe_3GaTe_2 (~ 40 nm) flake shows the same above-room-temperature T_C and a smaller coercivity (Fig. S1). The high T_C , large coercivity, and robust PMA make the Fe_3GaTe_2 flake an ideal metallic ferromagnetic electrode for MTJs working at room temperature [35].

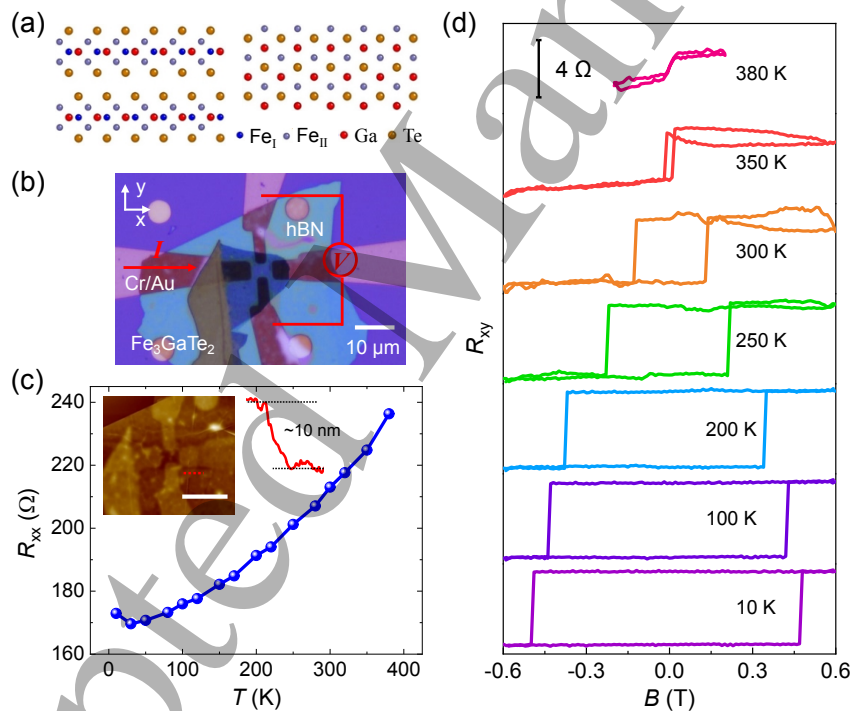


Figure 1: (a) Side (left) and top views (right) of the crystal structure of Fe_3GaTe_2 . (b) The optical image of a Fe_3GaTe_2 Hall-bar device capped by hBN. Scale bar: $10 \mu\text{m}$. The direction of the current and the connection of the voltmeter during Hall measurements are shown in red. (c) Longitudinal resistance R_{xx} versus temperature from 10 to 380 K. Upper-left inset: AFM image and height profile of the Fe_3GaTe_2 . Scale bar: $10 \mu\text{m}$. (d) Hall resistance R_{xy} versus perpendicular magnetic field (B) of a ~ 10 nm thick Fe_3GaTe_2 at different temperatures ranging from 10 to 380 K. The bias current I_{xx} is fixed at $10 \mu\text{A}$.

We now focus on the fabrication and properties of the MTJ. Figures 2a-b show the schematic and optical image of the two-terminal MTJ. Here, two metallic Fe_3GaTe_2 ferromagnetic electrodes are separated by a non-magnetic WSe_2 spacer layer. The whole structure is capped with a hBN layer (typically 10-30 nm) to prevent degradation or oxidation once the MTJ is exposed to air (details of the fabrication in Supplementary Note 1). The semiconductor 2H- WSe_2 is a typical TMDC material in a hexagonal structure with space group $P6_3/mmc$, consisting of van der Waals bonded Se-W-Se layers [37]. The bulk WSe_2 is an indirect-gap semiconductor with a band gap of 1.20 eV, while WSe_2 has a direct band gap of 1.65 eV in its monolayer form [38]. The AFM study of the MTJ indicates that the thickness of the spacer WSe_2 layer is ~ 7 nm (inset of Fig. 2b). To distinguish the coercivities of the top and bottom ferromagnetic electrodes in the MTJs, we selected Fe_3GaTe_2 flakes with different thicknesses (~ 11 nm bottom Fe_3GaTe_2 and ~ 17 nm top Fe_3GaTe_2). The different switching fields of the top and bottom ferromagnetic layers enable the parallel and antiparallel configurations under different specific magnetic fields, corresponding to the low and high resistance states of the MTJ [39]. Raman spectroscopy was used to characterize the Fe_3GaTe_2 and WSe_2 layers. The WSe_2 layer has a room temperature photoluminescence (PL) emission centred at 1.38 eV (Fig. S2), in good agreement with previous experimental results [35, 40]. The preliminary studies indicate a high-quality WSe_2 spacer layer, as required to preserve the polarization of the electron as it tunnels in the MTJ [17].

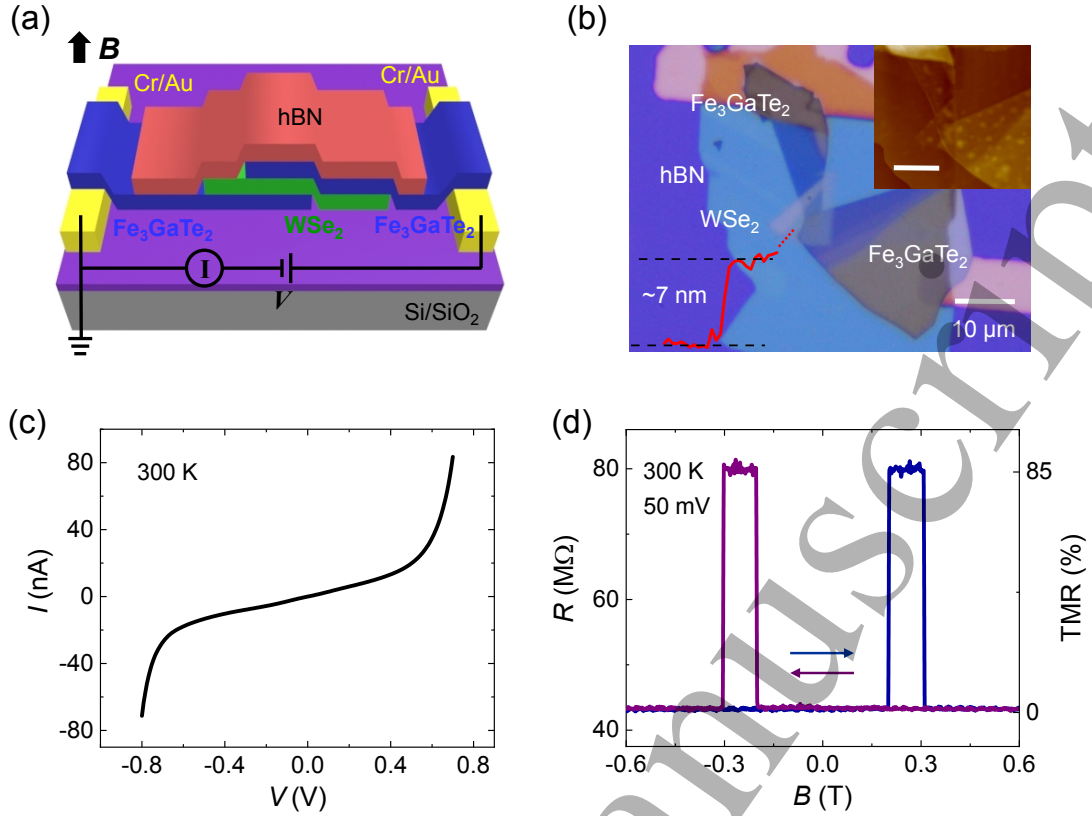


Figure 2: (a) Schematic of Fe₃GaTe₂/WSe₂/Fe₃GaTe₂ MTJs. (b) Optical image and AFM image (upper-right inset) of a representative Fe₃GaTe₂/WSe₂/Fe₃GaTe₂ heterojunction device encapsulated by a top hBN layer. Scale bar: 10 μm. The lower-left inset shows the height profile of the spacer layer WSe₂. (c) I - V characteristics of the device at $T = 300$ K. (d) Room temperature resistance (R) and TMR versus perpendicular magnetic field (B) of the device at a constant bias voltage $V = 50$ mV.

Figure 2c shows a symmetric, nonlinear I - V curve of the device, which point to typical tunneling behaviour [26, 31]. By applying a constant bias voltage ($V = 50$ mV) and sweeping the perpendicular magnetic field (B), we observed a sharp jump of the resistance from low (R_p) to high-resistance state (R_{AP}) at $B = 0.20$ T (Fig. 2d). With further increasing B to 0.31 T, the resistance jumps back to the low-resistance state. Symmetric resistance jumps are also observed for sweeping B from positive to negative values. The distinct low- and high-resistance states correspond to the magnetization of the two Fe₃GaTe₂ layers in the parallel ($\downarrow\downarrow$ or $\uparrow\uparrow$) and antiparallel ($\downarrow\uparrow$ or $\uparrow\downarrow$) magnetization configurations, respectively. In the parallel configuration, spin-dependent tunneling occurs between the same spin states, representing R_p with the product

of the DOS of the majority (D_{\uparrow}) and minority (D_{\downarrow}) spins as $1/R_P \propto (D_{\uparrow} \times D_{\uparrow}) + (D_{\downarrow} \times D_{\downarrow})$ [30]. In the antiparallel configuration, R_{AP} is conversely determined by the cross product of the DOS with different spin states as $1/R_{AP} \propto 2D_{\uparrow} \times D_{\downarrow}$, leading to a larger R_{AP} for MTJs under low bias voltages [30]. At $V = 50$ mV and $T = 300$ K, the R_P and R_{AP} of the junction are 43.3 M Ω and 80.4 M Ω , respectively. The corresponding $TMR = (R_{AP} - R_P)/R_P$ is 85% , even higher than that of some reported conventional MTJs working at room temperature, such as Fe/Al₂O₃/Fe (TMR = 18% , [41]) and Fe/MgO/Fe (TMR = 30% , [42]). Similar results were obtained in another device displaying a TMR of 53% at room temperature (Fig. S3). Thus, the room-temperature TMR in our devices is an important achievement, filling a gap in the current literature on TMR in all-2D vdW MTJs.

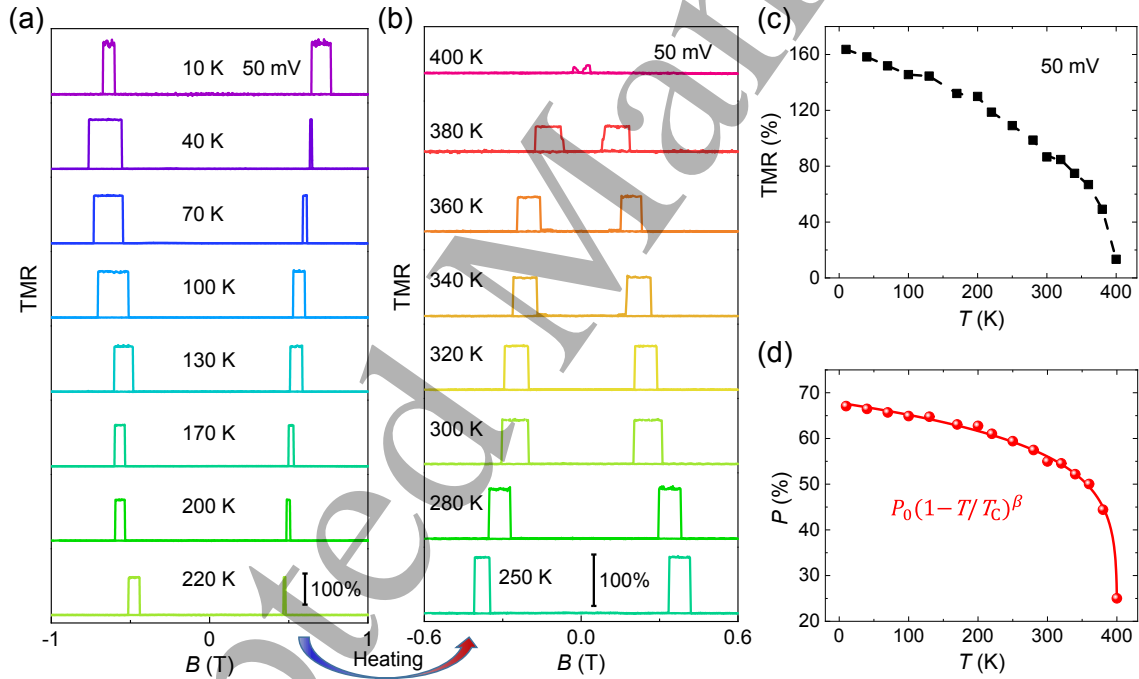


Figure 3: (a-b) R and TMR versus B of the device at different temperatures ranging from 10 to 400 K. (c) TMR versus temperature of the device at $V = 50$ mV. The values of TMR are derived from (a-b). (d) Spin polarization (P) versus temperature of the device. The fitting curve follows the function of $P = P_0(1-T/T_C)^\beta$.

Figures 3a-b show the TMR curves measured at various temperatures. A TMR of 164% in the device is observed at $T = 10$ K, while another device exhibits a larger TMR of 210% at

the same temperature (Fig. S4). With increasing temperature, the magnitude of the TMR decreases and vanishes above T_C (Fig. 3c). The spin polarization is proportional to the magnetization and decreases with increasing temperature [43], thus leading to a smaller TMR. Moreover, due to the reduction of perpendicular anisotropic energy and the enhancement of thermal energy, the coercivity of Fe_3GaTe_2 decreases with increasing temperature as well [43]. This is reflected by the reduction of the critical magnetic switching field of the MTJ in Figs. 3a-b. Interestingly, some TMR – V curves in Fig. 3a are asymmetric, indicating that the coercivity of Fe_3GaTe_2 can be different at positive and negative magnetic field. This can be attributed to the defect-related pinning effect, which is weakened at high temperatures (Fig. 3b) [44]. The TMR can be defined as $\text{TMR} = 2P^2/(1 - P^2)$, where $P = (D_{\uparrow} - D_{\downarrow})/(D_{\uparrow} + D_{\downarrow})$ denotes the spin polarization at the Fermi-level (E_F) for the injector and detector Fe_3GaTe_2 electrodes [45]. A room-temperature spin polarization P of 55 % is calculated by the TMR of 85%. As shown in Fig. 3d, the estimated temperature-dependence of the spin polarization can be fitted well by a power-law given by $P = P_0(1-T/T_C)^\beta$, where P_0 is the spin polarization at 0 K and β is a material-dependent constant that can be fitted to $\beta = 0.137$ [46, 47]. Our fitting results also indicate that $T_C = 400$ K, which is close to that obtained in Fig. 3b. Another MTJ shown in Fig. S4 shows a similar behaviour, but with a lower T_C of 357 K (see Supplementary Note 2).

In summary, our results demonstrate that the vdW heterostructure $\text{Fe}_3\text{GaTe}_2/\text{WSe}_2/\text{Fe}_3\text{GaTe}_2$ provides an excellent platform for MTJs. It exhibits an ideal tunneling behaviour with a TMR signal as large as 85 % at room temperature, corresponding to a spin polarization of 55 %. The large room-temperature magnetoresistance is comparable to that of state-of-the-art conventional MTJs and represents a significant advance due to the absence of room-temperature TMR in all-2D MTJs. By adjusting the thickness of the spacer layer, the TMR could be further increased. Also, we envisage that the use of vdW tunnel barriers in Fe_3GaTe_2 -based MTJs, such as the wide-bandgap semiconductor GaSe or insulator

hBN, larger TMRs could be achieved, offering opportunities for further advances and new possibilities for next-generation spintronic devices.

Acknowledgment. This work was supported by the National Key Research and Development Program of China (Grant Nos. 2022YFA1405100 and 2022YFE0134600), the Beijing Natural Science Foundation Key Program (Grant No. Z190007), the National Natural Science Foundation of China (Grant Nos. 61774144, 62005265, and 52272152), the Key Research Program of Frontier Sciences (Grant Nos. QYZDY-SSW-JSC020), the Strategic Priority Research Program of Chinese Academy of Sciences (Grant Nos. XDB44000000 and XDB28000000).

References

- [1] Yang H, Valenzuela S O, Chshiev M, Couet S, Dieny B, Dlubak B, Fert A, Garello K, Jamet M, Jeong D E, Lee K, Lee T, Martin M B, Kar G S, Seneor P, Shin H J and Roche S 2022 *Nature* **606** 663
- [2] Moodera J S, Kinder L R, Wong T M and Meservey R 1995 *Phys. Rev. Lett.* **74** 3273
- [3] Wang W-G, Li M, Hageman S and Chien C L 2011 *Nat. Mater.* **11** 64
- [4] Wang W, Narayan A, Tang L, Dolui K, Liu Y, Yuan X, Jin Y, Wu Y, Rungger I, Sanvito S and Xiu F 2015 *Nano Lett.* **15** 5261
- [5] Butler W H, Zhang X G, Schulthess T C and MacLaren J M 2001 *Phys. Rev. B* **63** 054416
- [6] Yuasa S, Nagahama T, Fukushima A, Suzuki Y and Ando K 2004 *Nat. Mater.* **3** 868
- [7] Kalitsov A, Zermatten P J, Bonell F, Gaudin G, Andrieu S, Tiusan C, Chshiev M and Velev J P 2013 *J. Phys. Condens. Matter* **25** 496005
- [8] Dorneles L S, Sommer R L and Schelp L F 2002 *J. Appl. Phys.* **91** 7971
- [9] Ning J, Zhou Y, Zhang J, Lu W, Dong J, Yan C, Wang D, Shen X, Feng X, Zhou H and Hao Y 2020 *Appl. Phys. Lett.* **117** 163104
- [10] Xie S, Shiffa M, Shiffa M, Kudrynskiy Z R, Makarovskiy O, Kovalyuk Z D, Zhu W, Wang K and Patanè A 2022 *npj 2D Mater. Appl.* **6** 61
- [11] Gong C, Li L, Li Z, Ji H, Stern A, Xia Y, Cao T, Bao W, Wang C, Wang Y, Qiu Z Q, Cava R J, Louie S G, Xia J and Zhang X 2017 *Nature* **546** 265

- [12] Huang B, Clark G, Navarro-Moratalla E, Klein D R, Cheng R, Seyler K L, Zhong D, Schmidgall E, McGuire M A, Cobden D H, Yao W, Xiao D, Jarillo-Herrero P and Xu X 2017 *Nature* **546** 270
- [13] Huang B, Clark G, Klein D R, MacNeill D, Navarro-Moratalla E, Seyler K L, Wilson N, McGuire M A, Cobden D H, Xiao D, Yao W, Jarillo-Herrero P and Xu X 2018 *Nat. Nanotechnol.* **13** 544
- [14] Fei Z, Huang B, Malinowski P, Wang W, Song T, Sanchez J, Yao W, Xiao D, Zhu X, May A F, Wu W, Cobden D H, Chu J H and Xu X 2018 *Nat. Mater.* **17** 778
- [15] Deng Y, Yu Y, Song Y, Zhang J, Wang N Z, Sun Z, Yi Y, Wu Y Z, Wu S, Zhu J, Wang J, Chen X H and Zhang Y 2018 *Nature* **563** 94
- [16] May A F, Ovchinnikov D, Zheng Q, Hermann R, Calder S, Huang B, Fei Z, Liu Y, Xu X and McGuire M A 2019 *ACS Nano* **13** 4436
- [17] Hu C, Zhang D, Yan F, Li Y, Lv Q, Zhu W, Wei Z, Chang K and Wang K 2020 *Sci. Bull.* **65** 1072
- [18] Ye X-G, Zhu P-F, Xu W-Z, Shang N, Liu K and Liao Z-M 2022 *Chin. Phys. Lett.* **39** 037303
- [19] Feng H, Li Y, Shi Y, Xie H-Y, Li Y and Xu Y 2022 *Chin. Phys. Lett.* **39** 077501
- [20] Liu S, Yuan X, Zou Y, Sheng Y, Huang C, Zhang E, Ling J, Liu Y, Wang W, Zhang C, Zou J, Wang K and Xiu F 2017 *npj 2D Mater. Appl.* **1** 30
- [21] Kim K, Seo J, Lee E, Ko K T, Kim B S, Jang B G, Ok J M, Lee J, Jo Y J, Kang W, Shim J H, Kim C, Yeom H W, Il Min B, Yang B J and Kim J S 2018 *Nat. Mater.* **17** 794
- [22] Albarakati S, Tan C, Chen Z-J, Partridge James G, Zheng G, Farrar L, Mayes Edwin L H, Field Matthew R, Lee C, Wang Y, Xiong Y, Tian M, Xiang F, Hamilton Alex R, Tretiakov Oleg A, Culcer D, Zhao Y-J and Wang L 2019 *Sci. Adv.* **5** eaaw0409
- [23] Alghamdi M, Lohmann M, Li J, Jothi P R, Shao Q, Aldosary M, Su T, Fokwa B P T and Shi J 2019 *Nano Lett.* **19** 4400
- [24] Ding B, Li Z, Xu G, Li H, Hou Z, Liu E, Xi X, Xu F, Yao Y and Wang W 2019 *Nano Lett.* **20** 868
- [25] Lin H, Yan F, Hu C, Lv Q, Zhu W, Wang Z, Wei Z, Chang K and Wang K 2020 *ACS Appl. Mater. Interfaces* **12** 43921
- [26] Zhu W, Lin H, Yan F, Hu C, Wang Z, Zhao L, Deng Y, Kudrynskiy Z R, Zhou T, Kovalyuk Z D, Zheng Y, Patané A, Žutić I, Li S, Zheng H and Wang K 2021 *Adv. Mater.* **33** 2104658

- [27] Zheng Y, Ma X, Yan F, Lin H, Zhu W, Ji Y, Wang R and Wang K 2022 *npj 2D Mater. Appl.* **6** 62
- [28] Lin H, Yan F, Hu C, Zheng Y, Sheng Y, Zhu W, Wang Z, Zheng H and Wang K 2022 *Nanoscale* **14** 2352
- [29] Kao I H, Muzzio R, Zhang H, Zhu M, Gobbo J, Yuan S, Weber D, Rao R, Li J, Edgar J H, Goldberger J E, Yan J, Mandrus D G, Hwang J, Cheng R, Katoch J and Singh S 2022 *Nat. Mater.* **21** 1029
- [30] Min K-H, Lee D H, Choi S-J, Lee I-H, Seo J, Kim D W, Ko K-T, Watanabe K, Taniguchi T, Ha D H, Kim C, Shim J H, Eom J, Kim J S and Jung S 2022 *Nat. Mater.* **21** 1144
- [31] Wang Z, Sapkota D, Taniguchi T, Watanabe K, Mandrus D and Morpurgo A F 2018 *Nano Lett.* **18** 4303
- [32] Li Z, Tang M, Huang J, Qin F, Ao L, Shen Z, Zhang C, Chen P, Bi X, Qiu C, Yu Z, Zhai K, Ideue T, Wang L, Liu Z, Tian Y, Iwasa Y and Yuan H 2022 *Adv. Mater.* **34** 2201209
- [33] Cao Y, Zhang X, Zhang X-P, Yan F, Wang Z, Zhu W, Tan H, Golovach V N, Zheng H and Wang K 2022 *Phys. Rev. Appl.* **17** L051001
- [34] Zhou H, Zhang Y and Zhao W 2021 *ACS Appl. Mater. Interfaces* **13** 1214
- [35] Zhang G, Guo F, Wu H, Wen X, Yang L, Jin W, Zhang W and Chang H 2022 *Nat. Commun.* **13** 5067
- [36] Gong K, Zhang L, Liu D, Liu L, Zhu Y, Zhao Y and Guo H 2014 *Nanotechnology* **25** 435201
- [37] Kumar A and Ahluwalia P K 2012 *Eur. Phys. J. B* **85** 186
- [38] Pudasaini P R, Oyedele A, Zhang C, Stanford M G, Cross N, Wong A T, Hoffman A N, Xiao K, Duscher G, Mandrus D G, Ward T Z and Rack P D 2017 *Nano Res.* **11** 722
- [39] Bowen M, Cros V, Petroff F, Fert A, Martínez Boubeta C, Costa-Krämer J L, Anguita J V, Cebollada A, Briones F, de Teresa J M, Morellón L, Ibarra M R, Güell F, Peiró F and Cornet A 2001 *Appl. Phys. Lett.* **79** 1655
- [40] Shi W, Lin M-L, Tan Q-H, Qiao X-F, Zhang J and Tan P-H 2016 *2D Mater.* **3** 025016
- [41] Miyazaki T and Tezuka N 1995 *J. Magn. Magn. Mater.* **139** L231
- [42] Tiusan C, Faure-Vincent J, Bellouard C, Hehn M, Jouguelet E and Schuhl A 2004 *Phys. Rev. Lett.* **93** 106602
- [43] Hu C, Yan F, Li Y and Wang K 2021 *Chin. Phys. B* **30** 097505
- [44] Dho J, Lee E K, Park J Y and Hur N H 2005 *J. Magn. Magn. Mater.* **285** 164
- [45] Žutić I, Fabian J and Das Sarma S 2004 *Rev. Mod. Phys.* **76** 323

[46] Wang X, Li D, Li Z, Wu C, Che C M, Chen G and Cui X 2021 *ACS Nano* **15** 16236

[47] Bedoya-Pinto A, Ji J-R, Pandeya A K, Gargiani P, Valvidares M, Sessi P, Taylor J M, Radu F, Chang K and Parkin S S P 2021 *Science* **374** 616

Accepted Manuscript

Supplementary Materials for

Large room-temperature magnetoresistance in van der Waals

ferromagnet/semiconductor junctions

Wenkai Zhu^{1,2,†}, Shihong Xie^{1,3,†}, Hailong Lin^{1,2,†}, Gaojie Zhang^{4,5}, Hao Wu^{4,5}, Tiangui Hu^{1,2},
Ziao Wang^{1,2}, Xiaomin Zhang^{1,2}, Jiahan Xu¹, Yujing Wang^{1,2}, Yuanhui Zheng¹, Faguang Yan¹,
Jing Zhang¹, Lixia Zhao^{1,6}, Amalia Patanè³, Jia Zhang^{5,7}, Haixin Chang^{4,5,*}, Kaiyou Wang^{1,2,*}

¹State Key Laboratory of Superlattices and Microstructures, Institute of Semiconductors, Chinese Academy of Sciences, Beijing 100083, China

²Center of Materials Science and Optoelectronics Engineering, University of Chinese Academy of Sciences, Beijing 100049, China

³School of Physics and Astronomy, University of Nottingham, Nottingham NG7 2RD, United Kingdom

⁴Center for Joining and Electronic Packaging, State Key Laboratory of Material Processing and Die & Mold Technology, School of Materials Science and Engineering, Huazhong University of Science and Technology, Wuhan 430074, China

⁵Wuhan National High Magnetic Field Center, Huazhong University of Science and Technology, Wuhan 430074, China

⁶School of Electrical and Electronic Engineering, Tiangong University, Tianjin 300387, China

⁷School of Physics, Huazhong University of Science and Technology, Wuhan 430074, China

[†]These authors contributed equally to this work.

*Authors to whom any correspondence should be addressed.

Email:

hxchang@hust.edu.cn

kywang@semi.ac.cn

Supplementary Note 1: Methods

Materials and device fabrication. The high-quality vdW bulk single-crystal WSe₂ and hBN were purchased from HQ Graphene, while Fe₃GaTe₂ was grown by the self-flux methods. To fabricate a Fe₃GaTe₂/WSe₂/Fe₃GaTe₂ MTJ, a Fe₃GaTe₂ flake was firstly exfoliated onto polydimethylsiloxane (PDMS) stamps by adhesive tape. Under an optical microscope, the Fe₃GaTe₂ flake with appropriate thickness and shape was chosen for transfer onto a 300 nm thick SiO₂/Si by using a position-controllable dry transfer method. Then, using the same method, a WSe₂ flake was transferred onto the Fe₃GaTe₂ flake, followed by another thicker Fe₃GaTe₂ flake to fabricate a vdW heterojunction. To prevent the Fe₃GaTe₂ from oxidation, a hBN layer was used to cap the whole heterostructure. Finally, the device was annealed at 120 °C for 10 minutes to reduce the bubbles between the layers and ensure close contact between the layers. Notably, the whole transfer processes were performed in a nitrogen-filled glovebox with a concentration of less than 0.1 ppm of oxygen and water to ensure a clean interface. The source and drain electrode regions were pre-patterned by standard photolithography, and Cr/Au (10/40 nm) layers were deposited using an ultrahigh vacuum magnetron sputtering system, followed by a lift-off process. By a similar process, a Fe₃GaTe₂/hBN heterostructure was stamped onto four pre-patterned Cr/Au (10/15 nm) electrodes on a 300 nm thick SiO₂/Si substrate to form a Hall-bar device. The electrodes of the Hall-bar device were patterned by standard electron beam lithography (EBL) and an ultrahigh vacuum magnetron sputtering, followed by a lift-off process.

Electrical, optical and microscopy measurements. The electrical measurements were carried out in a Model CRX-VF Cryogenic Probe Station (Lake Shore Cryotronics, Inc.) with a ±2.25 T out-of-plane perpendicular magnetic field. The instrument operation temperature varies from 10 to 400 K. The AHE was measured by the combination of Keithley model 2602B sourcemeter and Keithley model 2182 A nanovoltmeter. The electrical transport properties of MTJs were measured by a semiconductor characterization system (Agilent Technology

B1500A). The thickness of Fe_3GaTe_2 and WSe_2 flakes were determined by an AFM (Bruker Multimode 8). The $\text{Fe}_3\text{GaTe}_2/\text{WSe}_2/\text{Fe}_3\text{GaTe}_2$ device optical image was obtained using an Olympus optical microscope. Raman and photoluminescence spectra of WSe_2 and Fe_3GaTe_2 flakes were obtained by optical microscopy (Renishaw inVia-Reflex) with excitation by a 532 nm laser.

Accepted Manuscript

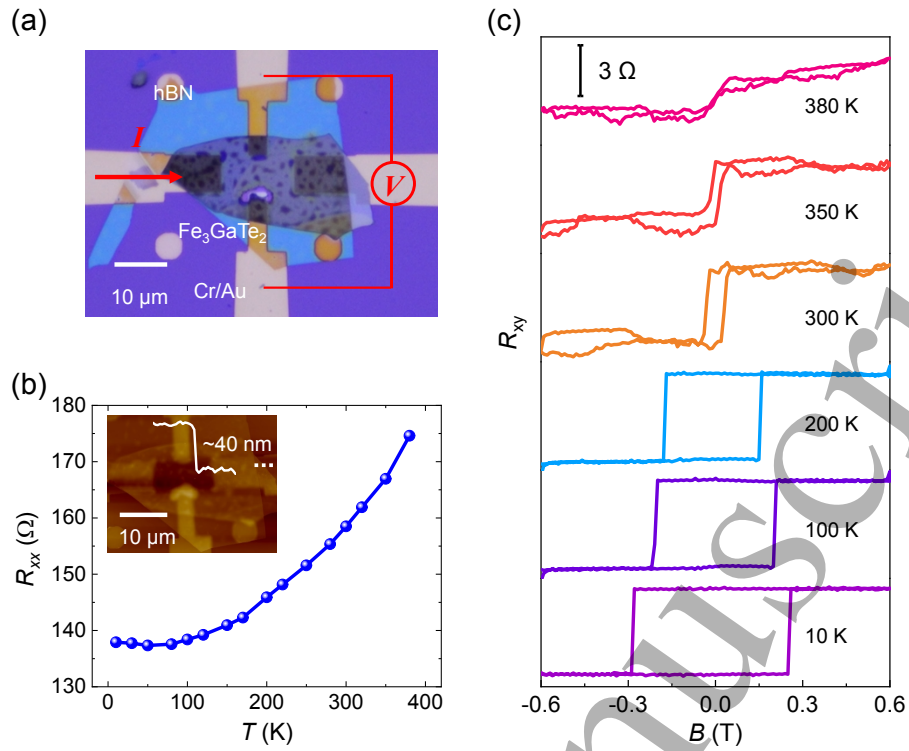


Figure S1: (a) The optical image of a thick (40 nm) Fe₃GaTe₂ Hall-bar device capped by hBN. Scale bar: 10 μm. The direction of the current and the connection of the voltmeter are shown in red. (b) Longitudinal resistance R_{xx} versus temperature from 10 to 380 K. Upper-left inset: AFM image and height profile of the Fe₃GaTe₂ Hall-bar device. Scale bar: 10 μm. (c) Hall resistance R_{xy} versus perpendicular magnetic field (B) at different temperatures ranging from 10 to 380 K. The bias current I_{xx} is fixed at 10 μA.

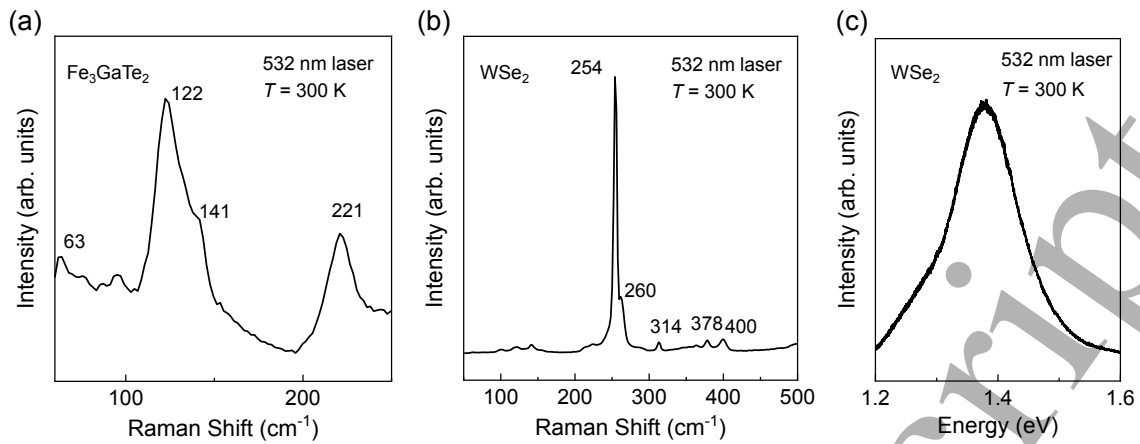


Figure S2: (a) Raman spectrum of a bulk Fe_3GaTe_2 flake ($T = 300 \text{ K}$, $\lambda = 532 \text{ nm}$). (b) Raman spectrum of a bulk WSe_2 flake ($T = 300 \text{ K}$, $\lambda = 532 \text{ nm}$). (c) Photoluminescence (PL) spectrum of a bulk WSe_2 flake ($T = 300 \text{ K}$, $\lambda = 532 \text{ nm}$). The spectrum shows the band edge emission of WSe_2 , which is centred at about 1.38 eV .

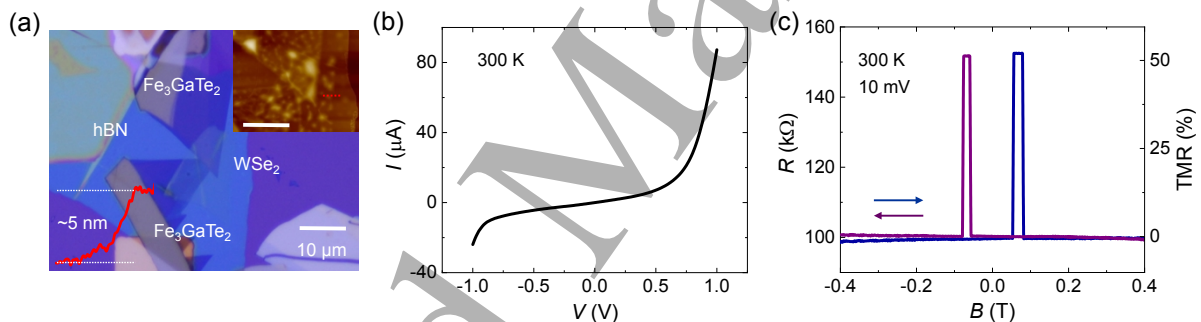


Figure S3: (a) Optical image and AFM image (upper right inset) of another $\text{Fe}_3\text{GaTe}_2/\text{WSe}_2/\text{Fe}_3\text{GaTe}_2$ MTJ device with a thin (5 nm) spacer layer. Scale bar: $10 \mu\text{m}$. Lower-left inset: the height profile of the spacer layer WSe_2 . (b) I - V characteristics of the device at $T = 300 \text{ K}$. (c) Room temperature R and TMR versus B at 10 mV bias.

Supplementary Note 2: Temperature-dependent TMR of another device

Figures S4a-b show the TMR curves of another device measured at various temperatures. An extremely large TMR of 210% in the device is observed at $T = 10$ K. Same as the device in the main text, the magnitude of the TMR decreases and vanishes above T_C with increasing temperature (Fig. S4c). Interestingly, the TMR of this device (210%, 10K) is larger than that of the device in the main text (164%, 10K) at a low temperature, but the TMR of this device (53%, 300K) is smaller than that of the device in the main text (85%, 300K) at room temperature, which indicates that the TMR of this device decays more significantly with increasing temperature. This is caused by the difference in T_C of Fe_3GeTe_2 between the two devices. Fitted by power-law $P = P_0(1-T/T_C)^\beta$ (Fig. S4d), we get a $T_C = 357$ K of Fe_3GeTe_2 in this device, which is lower than that of the device in the main text ($T_C = 400$ K). From the literature [S1], we know that the T_C of Fe_3GeTe_2 decreases monotonically with decreasing thickness. Thinner Fe_3GeTe_2 layers (~ 8 nm bottom layer and ~ 9 nm top layer) in this device lead to a lower T_C , resulting in a smaller TMR at room temperature.

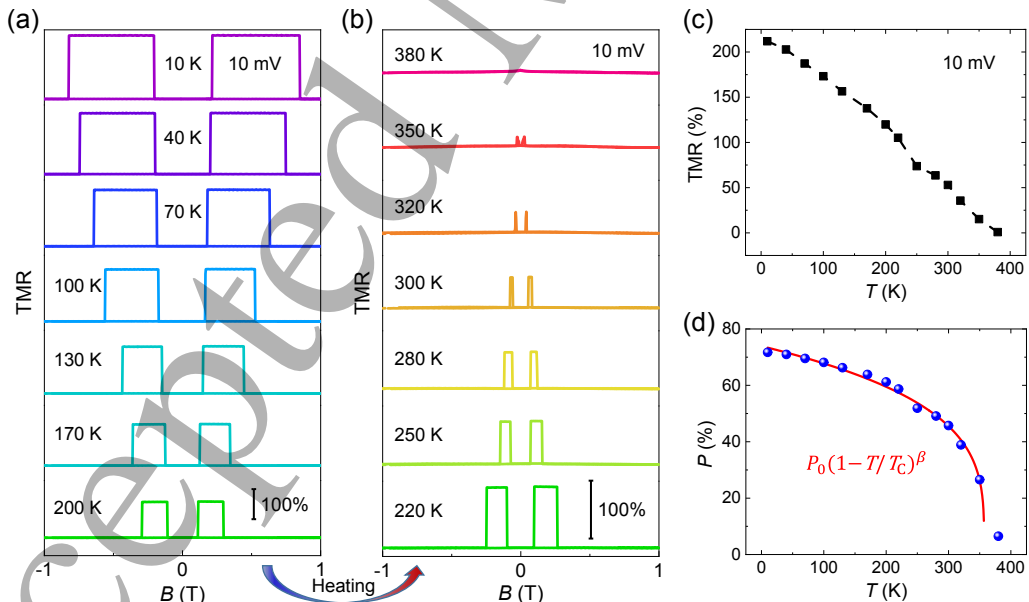


Figure S4: (a-b) R and TMR versus B of another device at different temperatures ranging from 10 to 380 K. (c) TMR versus temperature of the device at $V = 10$ mV. The values of TMR are obtained from parts (a-b). (d) Spin polarization (P) versus temperature of the device. The fitting curve follows the form of $P = P_0(1-T/T_C)^\beta$.

Reference

[S1] Zhang G, Guo F, Wu H, Wen X, Yang L, Jin W, Zhang W and Chang H 2022 *Nat. Commun.* **13** 5067

Accepted Manuscript